

**Titre:** Sodium alginate-grafted submicrometer particles display enhanced reversible aggregation/disaggregation properties

**Auteurs:** Faezeh Sabri, Kevin Berthomier, Antoine Marion, Louis Fradette,  
Authors: Jason Robert Tavares, & Nick Virgilio

**Date:** 2018

**Type:** Article de revue / Article

**Référence:** Sabri, F., Berthomier, K., Marion, A., Fradette, L., Tavares, J. R., & Virgilio, N. (2018). Sodium alginate-grafted submicrometer particles display enhanced reversible aggregation/disaggregation properties. Carbohydrate Polymers, 194, 61-68. <https://doi.org/10.1016/j.carbpol.2018.04.012>

## Document en libre accès dans PolyPublie

Open Access document in PolyPublie

**URL de PolyPublie:** <https://publications.polymtl.ca/3734/>  
PolyPublie URL:

**Version:** Version finale avant publication / Accepted version  
Révisé par les pairs / Refereed

**Conditions d'utilisation:** Creative Commons Attribution-Utilisation non commerciale-Pas d'oeuvre dérivée 4.0 International / Creative Commons Attribution-NonCommercial-NoDerivatives 4.0 International (CC BY-NC-ND)  
Terms of Use:

## Document publié chez l'éditeur officiel

Document issued by the official publisher

**Titre de la revue:** Carbohydrate Polymers (vol. 194)  
Journal Title:

**Maison d'édition:** Elsevier  
Publisher:

**URL officiel:** <https://doi.org/10.1016/j.carbpol.2018.04.012>  
Official URL:

**Mention légale:** © 2018. This is the author's version of an article that appeared in Carbohydrate Polymers (vol. 194) . The final published version is available at <https://doi.org/10.1016/j.carbpol.2018.04.012>. This manuscript version is made available under the CC-BY-NC-ND 4.0 license <https://creativecommons.org/licenses/by-nc-nd/4.0/>  
Legal notice:

1 Sodium Alginate-Grafted Submicrometer Particles

2 Display Enhanced Reversible

3 Aggregation/Disaggregation Properties

4 *Faezeh Sabri, Kevin Berthomier, Antoine Marion, Louis Fradette, Jason R. Tavares*

5 *and Nick Virgilio\**

6 <sup>a</sup> Center for Applied Research on Polymers and Composites (CREPEC), Department of

7 Chemical Engineering, Polytechnique Montréal, Montréal, Québec, H3C 3A7, Canada

8

9 \* Corresponding author:

10 Phone: 1-514-340-4711 #4524

11 Fax: 1-514-340-4159

12 Email address: [nick.virgilio@polymtl.ca](mailto:nick.virgilio@polymtl.ca)

13 Postal address: Department of Chemical Engineering, Polytechnique Montréal, C.P. 6079

14 Succursale Centre-Ville, Montréal, Québec, H3C 3A7

15

16

17

**ABSTRACT.** In this article, we demonstrate that submicrometer particles with surface-grafted sodium alginate (SA) display enhanced and reversible aggregation/disaggregation properties in aqueous solution. 300 nm silica particles were first functionalized with an aminosilane coupling agent, followed by the grafting of pH-sensitive SA, as confirmed by zeta potential, XPS and FTIR analyses. The SA-modified particles show enhanced aggregation properties at acidic pH compared to unmodified silica, with a 10 times increase in average aggregate diameter. The process is reversible, as the aggregates can be broken and dispersed again when the pH is increased back to 7.0. As a result, the sedimentation rate of SA-modified particles at pH 3.0 is both significantly faster and complete compared to the unmodified particles. This enhanced aggregation is most likely due to the formation of intermolecular hydrogen bonds between neighboring SA-modified particles. This work illustrates how surface-grafted macromolecules of natural origins can be used to tune interparticle interactions, in order to improve separation processes.

**KEYWORDS:** submicrometer particle, surface modification, sodium alginate, pH sensitive, aggregation.

## 1. Introduction

The controlled aggregation and dispersion of colloids is a key step in separation processes involving complex fluids comprised of immiscible liquids and/or micro/nanoparticles (*e.g.* Pickering emulsions), in fields such as petrochemistry (Doshi, Repo, Heiskanen, Sirvio, & Sillanpaa, 2017; Hosseini et al., 2016; Mohammadi, Rashidi, Mousavi-Dehghani, & Ghazanfari, 2016) and waste water treatment (Bakhteeva et al., 2016; Chai et al., 2015; Leudjo Taka, Pillay, & Yangkou Mbianda, 2017). When particle separation is required, it is often desirable to form aggregates and flocs as large as possible, in order to ease the separation process and decrease costs. Furthermore, if those particles were originally added to the process, for example as supports for much smaller catalytic nanoparticles (Ballauff & Lu, 2007), reversible aggregation/disaggregation behavior would be a desirable feature for recycling purpose.

The Derjaguin–Landau–Verwey–Overbeek (DLVO) theory is a classical framework to understand and analyze the stability of colloidal suspensions (Chin, Yiacoumi, & Tsouris, 2001; Ohki & Ohshima, 1999). It models particle-particle interactions as a combination of repulsive double-layer overlap forces and attractive dispersion (van der Waals) forces (Verwey, 1947). In the energy landscape, the contribution of the electrostatic repulsion superimposes to the Van der Waals attraction and generates an energy barrier that can reduce or inhibit particle aggregation in a suspension (Rodgers, Velicky, & Dryfe, 2015). Other forces that can also enhance or inhibit aggregation include the hydrophobic effect, hydrogen bonding, steric interactions, and depletion forces (Durand-Gasselin, Sanson, & Lequeux, 2011). As a result, the typical ways to control the aggregation level of micro/nanoparticles in a suspension are via pH and/or ionic strength (salt addition) adjustments (Yan et al., 2013), which control the electrical double layer properties. Grafting water-soluble polymer/polyelectrolyte chains on particle surface, which promote

stabilization via steric interactions (Hemraz, Lu, Sunasee, & Boluk, 2014), and/or adding polyelectrolytes (Borkovec & Papastavrou, 2008) or water-soluble macromolecules (Bakumov & Kroke, 2008) are two other approaches.

Recently, nanoparticles responding reversibly to external stimuli, such as changes in pH (Chen et al., 2017; Jia et al., 2016; Stular, Jerman, Naglic, Simoncic, & Tomsic, 2017; Xu et al., 2015) or temperature (Abreu et al., 2016; Qiao, Niu, Wang, & Cao, 2010), have generated an interest for chemical engineering processes, drug delivery and biomedical applications. For example, thermo- and pH-sensitive particles have been employed to stabilize (Kawaguchi, 2007; Morelli, Holdich, & Dragosavac, 2016) and destabilize Pickering emulsions (Binks, Murakami, Armes, & Fujii, 2005) – allowing separation of the liquid constituents. They were also used as carriers for  $\approx 1$ -10 nm catalytic nanoparticles, easing their separation and recovery process (Ballauff & Lu, 2007). However, separating particles from a liquid phase remains an energy intensive process. As a result, the formation of flocs or aggregates facilitates separation and, if reversible, allows re-dispersion for multiple reuse.

We hypothesize that grafting sodium alginate (SA) polymer chains onto the surface of submicrometer particles can increase interparticle interactions and enhance their aggregation properties reversibly, since SA undergoes reversible gelling at low pH due to the protonation of its carboxylate groups and the formation of intermolecular hydrogen bonding. The main objective of this work is to design, synthesize and evaluate the stabilization and aggregation properties of model submicrometer silica particles modified with SA, and to compare the results to unmodified particles in order to confirm if the aggregation/disaggregation process is enhanced.

## 2. Experimental Section

### 2.1 Materials

Sub- $\mu\text{m}$  silica particles (SP) were supplied by Nippon Shokubai Trading Co., Ltd (average diameter  $d = 290 \pm 13.2$  nm by SEM, see Supporting Information **Figure S1**; specific surface area  $S = 42 \pm 2$   $\text{m}^2\cdot\text{g}^{-1}$ , measured by BET with an ASAP 2020 instrument from Micromeritics Instrument Corporation). Sodium alginate (SA) from brown algae was supplied by Sigma-Aldrich (CAS. 9005-38-3, low viscosity, molecular weight  $\approx 60$  kDa,  $\text{pK}_a = 3.5$ ) (Harnsilawat, Pongsawatmanit, & McClements, 2006). The M/G ratio ( $= 1.83$ ) was measured at  $80^\circ\text{C}$  with a  $10\text{ mg}\cdot\text{ml}^{-1}$  solution in  $\text{D}_2\text{O}$  for the  $^1\text{H}$  NMR using a Bruker Avance 500 instrument (11.7 T) at a frequency of 500 MHz (Rahelivao, Andriamanantoanina, Heyraud & Rinaudo, 2013). 128 scans using 32 000 data points were acquired with a relaxation time (D1) of 5 s, a 4 kHz spectral window and a  $30^\circ$  impulsion. (3-Aminopropyl) trimethoxysilane (APTMS, 97%), *N*-(3-Dimethylaminopropyl)-*N'*-ethylcarbodiimide hydrochloride (EDC,  $> 98\%$ ), *N*-Hydroxysuccinimide (NHS, 98%) and urea ( $> 98\%$ ) were all purchased from Sigma-Aldrich and used without further purification. Ethanol (99.8%) was obtained from Thermo Fisher Scientific. HCl 1N and NaOH 12N solutions were of analytical grade and prepared without further purification with Milli-Q water (DI water,  $18.2\ \Omega$ , Synergy 185 system by Fisher Scientific).

### 2.2 Particle Surface Modification

#### 2.2.1 Silane Coating Grafting

In order to graft SA on silica sub- $\mu\text{m}$  particles, a silane coupling agent was first covalently grafted on its surface. In a typical batch, 10 g of SP particles were added in a hydrophobized Erlenmeyer flask containing 100 ml of a 95% v/v ethanol solution and DI water, while stirring at 600-700 rpm with a magnetic stirrer (Arkles, 2006). The pH was then adjusted to 4.5 - 5.5 using HCl 1N.

APTMS was then added dropwise while stirring at room temperature, following three targeted surface concentrations: 0.01 (SP-A), 0.1 (SP-B) and 1 (SP-C) APTMS molecule·nm<sup>-2</sup> (based on particle specific surface) (Pickering, Khimi, & Ilanko, 2015). For example, to treat 10 g of particles with a desired surface APTMS density of 1 molecule·nm<sup>-2</sup> (SP-C), 0.131 ml of APTMS was added to the reaction medium. The reaction was then carried for 12 h. The particles were collected by centrifugation (Sorvall RC 6+, Thermo Fisher Scientific) at 8000 rpm for 15 min, and cleaned by washing twice with ethanol in order to rinse off any remaining unreacted silane. The particles were finally dried in a vacuum oven at 70 °C for 2 hrs.

### 2.2.2 Sodium Alginate Grafting

A fraction of the APTMS modified SPs were further modified by grafting SA using two different solution concentrations (**Table 1**): 0.1% (1) and 1% (2) w/v. As an example, following this terminology, SP-C-2 particles were modified with a silane coating targeting an APTMS surface density of 1 APTMS molecule·nm<sup>-2</sup>, followed by grafting of SA with a 1% w/v solution. In a typical experiment for the preparation of SP-((B-2) or (C-2)) particles, 0.2 g of SA was first dissolved in 20 ml of DI water (1% w/v). 0.29 g of EDC and 0.17 g of NHS (EDC/NHS molar ratio = 1) were then added to the solution (EDC/-COOH molar ratio = 0.5, relative to the -COOH groups of alginate) (Giani, Fedi, & Barbucci, 2012). Then, 2 g of APTMS modified SPs were added to the mixture and the pH was adjusted to 4.5 with HCl 1N. The reaction proceeded for 15 hrs at room temperature and the mixture was subsequently centrifuged at 8000 rpm to collect the modified particles, which were washed with DI water 3 times. Finally, the particles were dried in a vacuum oven at 70 °C for 10 hrs. The synthesis conditions of the surface-modified SPs are summarized in **Table 1**.

**Table 1.** Synthesis conditions of surface modified particles with APTMS and SA

Particle ID	Targeted APTMS density (molecule·nm <sup>-2</sup> )	APTMS (ml) <sup>a</sup>	EDC <sup>b</sup> (g)	NHS <sup>b</sup> (g)	SA solution concentration/volume <sup>b</sup> ((%w/v)/ml)
SP-A	0.01	1.31×10 <sup>-3</sup>	-	-	-
SP-B	0.1	1.31 ×10 <sup>-2</sup>	-	-	-
SP-C	1	1.31×10 <sup>-1</sup>	-	-	-
SP-A-1	0.01	1.31×10 <sup>-3</sup>	0.29×10 <sup>-2</sup>	0.17×10 <sup>-2</sup>	0.1/20
SP-B-2	0.1	1.31×10 <sup>-2</sup>	0.29×10 <sup>-1</sup>	0.17×10 <sup>-1</sup>	0.1/20
SP-C-2	1	1.31×10 <sup>-1</sup>	0.29	0.17	1/20

<sup>a</sup>For the modification of 10 g of silica particles (SP) with (3-Aminopropyl)trimethoxysilane (APTMS); <sup>b</sup>For 2 g of APTMS-grafted SP with *N*-(3-Dimethylaminopropyl)-*N*'-ethylcarbodiimide hydrochloride (EDC) and *N*-Hydroxysuccinimide (NHS).

## 2.3 Particle Surface Characterization

### 2.3.1 Zeta Potential Measurements

Particle zeta potential ( $\zeta$ ) was measured with a Zetasizer Nano ZSP instrument (Malvern Instruments Ltd., Worcestershire, UK). Samples were dispersed in DI water at pH 7.0 (adjusted by adding NaOH 12N), and the measurements were performed at 25 °C.  $\zeta$  after modification with APTMS and SA, at different pHs (3.0, 7.0 and 10.0), were measured on at least three different samples by microelectrophoresis at a particle concentration of 0.001 g·ml<sup>-1</sup>. Disposable zeta potential folded capillary cells (DTS1070) were used and all samples tested were freshly prepared. The instrument determined the electrophoretic mobility, and the Smoluchowski model was then applied by the software for the calculation of  $\zeta$  (Lattuada & Hatton, 2007).

### 2.3.2 High-resolution X-ray Photoelectron Spectroscopy (XPS) Analysis

Elemental analyses of unmodified and modified silica particles with APTMS were realized with a VG ESCALAB 3 MKII X-ray photoelectron spectroscope (XPS) equipped with a non-monochromatic Mg K $\alpha$  radiation source operated at 300 W (15 kV, 20 mA). XPS analyses were conducted to detect electrons with a takeoff angle normal to the surface of the sample, yielding a probed depth around 10 nm. The pass energy was 100 eV for survey scans and 20 eV for high-resolution scans, at 1.00 and 0.05 eV increments, respectively. The pressure during analysis was kept under  $5 \times 10^{-9}$  Torr ( $6.67 \times 10^{-11}$  Pa). Particles were stored under vacuum overnight prior to analysis. The results were analyzed using the Advantage XPS software package. The elemental distribution of the samples was determined on the basis of peak area comparison (C1s, O1s, etc.), normalized to their corresponding sensitivity factors, after the removal of the scattered electron background. In the case of higher resolution spectra, binding energies were referenced to the C1s peak at 285.0 eV to adjust for possible charging effects, and the Shirley method was applied for background noise subtraction. According to the data trend for each distribution of binding energy, the baseline was manually placed. Each curve is represented by its maximum binding energy (BE) in the Supporting information (**Figure S2**). The species' elemental distributions are obtained via Gaussian/Lorentzian curve fitting on the original curve. The number of sub-curves and their corresponding species were obtained with full width at half maximum (fwhm) = 1.6, 1.8, 2.2, and 2.4 eV for C, O, Si, and N, respectively.

### **2.3.3 Fourier Transform Infrared (FTIR) Spectroscopy Analysis**

A Perkin Elmer Spectrum 65 FTIR spectrometer operating in attenuated total reflectance mode (Zn/Se crystal) in the range of 650-4000 cm<sup>-1</sup> was used to characterize unmodified SiO<sub>2</sub> sub- $\mu$ m particles, as well as modified particles with APTMS and SA. For each sample, 32 scans were

recorded at a resolution of  $4\text{ cm}^{-1}$ . The spectra of SP, SP-C and SP-C-2 are presented as Supporting Information (**Figure S3**).

## **2.4 Characterization of Aggregation and Disaggregation Properties**

### **2.4.1 Visual Inspection of Sedimentation Kinetics**

0.2 g of each particle type was dispersed in 10 ml of DI water using an ultrasonic homogenizer equipped with a microtip (Cole-Parmer, instrument model CP505, 500 watts) at an amplitude of 20 % for 1 min (approximately  $60\text{ J}\cdot\text{ml}^{-1}$ ). The pH was then adjusted to 3.0 with HCl 1N when required. Particle sedimentation was monitored by taking photographs (Nikon DX equipped with an AF-S DX NIKKOR 18-55mm f/3.5-5.6G VRII objective) every 3 min after dispersion, for a total duration of 60 min. For all particle types, three samples were tested.

### **2.4.2 Optical Microscopy Observations**

Unmodified and surface modified particles were observed by dark field optical microscopy (Olympus BX51 by Cytoviva, Objectives = 10x and 50x Plan Fluorite, and 60x UPL Fluorite Oil, and 100x UPL Fluorite Oil camera Q imaging, Retigna 2000R fast 1394, cooled color 12 bit). For each type of particle, 0.02 g of particles was dispersed in 2.0 ml of DI water at pH 7.0 using the ultrasonic homogenizer at a 20% amplitude for 1 min ( $\approx 300\text{ J}\cdot\text{ml}^{-1}$ ); the pH was subsequently adjusted to 3.0 with HCl 1N when required. Solutions were subsequently diluted by adding 3 droplets into 5 ml of water at the corresponding pH while stirring with a magnetic stirrer for 30 s at 600 rpm. Finally, three drops of freshly prepared samples were placed on microscope glass slides and observed at different locations and magnifications. The images were analyzed using the ImageJ software, to calculate the average size (Feret diameter) of the observed aggregates (between 200 and 4000 aggregates were analyzed for each condition).

### **2.4.3 Measurement of Sedimentation Rate by UV-Vis Spectroscopy**

UV-Vis transmittance measurements as a function of time were performed to determine the sedimentation rate of unmodified and surface modified particles, using a UV-Vis spectrometer (Model DH-2000 from Ocean Optics, 10 ms integration time). For each particle type, one concentration was analyzed ( $0.01 \text{ g}\cdot\text{ml}^{-1}$ ) at 2 different pHs (3.0 and 7.0), by dispersing the required amount of particles in 2 ml of DI water (pH 7.0) using an ultrasonic homogenizer, as described previously; the pH was subsequently adjusted to 3.0 with HCl 1N when required. Then, 1 ml of each sample was transferred into a disposable polystyrene cuvette with a 1 cm path length for transmittance measurements at 656 nm every 3 min for a total duration of 60 min. The height of the beam path was located at 1.3 cm from the bottom of the cuvette. For each particle type, the transmittance measurements were repeated 3 times. The spectral measurements were normalized with the DI water transmittance values at pH 3.0 and 7.0 respectively.

#### **2.4.4 Aggregation/Disaggregation Reversibility Evaluation**

Each sample was prepared by dispersing 0.01 g of particles (SP, SP-A or SP-A-1) in 1 ml of DI water at pH 7.0. UV-Vis transmittance at 656 nm was then measured as a function of time for 60 min, using 1 ml disposable polystyrene cuvettes. Subsequently, the sample was transferred back into a vial and the pH was adjusted to pH 3.0 with HCl 1N. The sample was again transferred into a disposable cuvette for transmittance measurements at 656 nm for 60 min. Once the experiment was completed, the sample was transferred back again into a vial and the pH was again brought back to 7.0 with NaOH 12.0N. The particles were next re-dispersed by ultrasonication (20% amplitude for 20 sec). This whole cycle process was repeated 4 times. The spectral measurements were normalized with DI water transmittance values at pH 3.0 and 7.0 respectively.

#### 2.4.5 Effect of urea on sodium alginate solubility as a function of pH

Two vials, each containing 10 ml of 0.05% (w/v) SA in DI water solution at pH 7.0, were prepared. Then, urea was added into one of the vial ( $1.0 \text{ mol}\cdot\text{l}^{-1}$ ), and the pH of both vials was adjusted to 3.0 with HCl 1N. Pictures were taken before and after pH adjustment.

### 3. Results

#### 3.1 Surface Modification Analyzed by Zeta Potential, XPS and FTIR

The particles zeta potential  $\zeta$  was measured as a function of pH for bare silica particles (SP), modified particles with APTMS (SP-A to C), and with SA (SP-(A-1), (B-2), and (C-2)) (Table 2).

**Table 2.**  $\zeta$  of silica particles: untreated (SP), APTMS treated (SP-A to C), and APTMS+SA treated particles (SP-(A-1), (B-2) and (C-2)), as a function of pH (3.0, 7.0 and 10.0).

Particle ID	$\zeta$ (mV)		
	pH = 3.0	pH = 7.0	pH = 10.0
SP	$5.7 \pm 0.8$	$-56.4 \pm 1.4$	$-57.0 \pm 1.4$
SP-A	$11.0 \pm 1.2$	$-58.4 \pm 1.1$	$-57.0 \pm 1.3$
SP-B	$49.4 \pm 4.7$	$24.7 \pm 0.7$	$-24.2 \pm 0.7$
SP-C	$52.1 \pm 1.4$	$13.3 \pm 0.3$	$8.4 \pm 0.4$
SP-A-1	$6.5 \pm 1.0$	$-50.9 \pm 1.1$	$-49.4 \pm 0.6$
SP-B-2	$3.4 \pm 0.8$	$-45.6 \pm 0.6$	$-45.1 \pm 1.6$
SP-C-2	$-0.8 \pm 0.3$	$-43.2 \pm 1.0$	$-43.8 \pm 1.4$

SP particles display a slightly positive  $\zeta$  at pH 3.0 that decreases to negative values at pHs 7.0 and 10.0. This behavior is expected due to the deprotonation of hydroxyl groups on the SP surface as the pH increases (Knoblich & Gerber, 2001). SP particles modified with APTMS (SP-A SP-B,

SP-C) generally display higher positive values at pH 3.0. Increasing the initial concentration of APTMS in solution results in an increasing positive  $\zeta$ , from +11.0 mV to +52.1 mV. At pH 3.0, SP-A particles present a similar behavior as compared to unmodified SP particles due to low APTMS surface density. For SP-B and SP-C,  $\zeta$  increases significantly (49.4 and 52.1 mV) due to the expected higher APTMS surface density, confirming grafting of APTMS. Grafting of APTMS was also confirmed by XPS, the spectra revealing two different components related to N-H bonds (revealed from the N1s peak using high resolution XPS), and one component related to C-N bonds. The component at a BE  $\cong$  399.8 eV corresponds to  $-\text{NH}_2$  and the component at BE  $\cong$  401.5 eV corresponds to  $-\text{NH}_3^+$  groups (see Supporting Information, **Figure S2**). Grafting of APTMS was independently confirmed by FTIR with the appearance of a band at  $1450\text{ cm}^{-1}$ , associated with N-H bond asymmetrical deformation vibration (**Figure S3**).

When the pH increases to 7.0 and 10.0,  $\zeta$  of SP-A, SP-B and SP-C all shift towards lower positive (almost neutral) or negative values. This is explained by (1) the significant deprotonation of surface bound hydroxyl groups, yielding negatively charged  $-\text{O}^-$  (Knoblich & Gerber, 2001), and (2) the gradual deprotonation of APTMS  $-\text{NH}_3^+$  groups.

At pH 3.0, SA modified particles (SP-A-1, SP-B-2 and SP-C-2) display nearly neutral  $\zeta$  values (slightly positive or negative). This behavior is due to the protonation of the SA carboxylic acid groups ( $\text{pK}_a = 3.5$ ) (Harnsilawat et al., 2006) – confirming grafting of SA with APTMS. At pH 7.0 and 10.0, SP-A-1, SP-B-2 and SP-C-2 particles display almost identical and nearly constant  $\zeta$  values. At pH 7.0,  $\zeta$  drops to negative values ranging from -43.2 mV to -50.9 mV, while at pH 10.0 it reaches nearly -50 mV. This is expected since at pH 7.0 and 10.0, above the  $\text{pK}_a$  of SA, the  $-\text{COOH}$  groups on the surface are deprotonated and become negatively charged, like a number of other polysaccharides (*e.g.* xanthan gum) (Wang, Natale, Virgilio, & Heuzey, 2016). Grafting of

SA was also confirmed by FTIR (see **Figure S3**). Observed bands at 1649 and 1460  $\text{cm}^{-1}$  were attributed to asymmetric and symmetric stretching vibrations of carboxylate  $-\text{COO}-$ . Finally, the disappearance of the N-H band at 1450  $\text{cm}^{-1}$  is attributed to the grafting of SA and the formation of N-C=O bonds.

Zeta potential measurements, XPS and FTIR analyses confirm graftings of the silane coupling agent and sodium alginate. The next section will look at the aggregation state of the particles as a function of pH and surface chemistry.

### 3.2 Particle aggregation behavior

**Figure 1** displays the aggregation behavior of SP, SP-A, and SP-A-1 particles at pH 3.0 and 7.0, respectively. At pH 3.0, unmodified SP particles tend to form small aggregates due to their slightly positive charge (**Figure 1a**), while at pH 7.0 they are almost individually dispersed (**Figure 1b**). These observations agree with the  $\zeta$  measurements reported in **Table 1**: at pH 3.0, the small positive value results in an unstable dispersion, while at pH 7.0, the significant negative value leads to a stable dispersion.

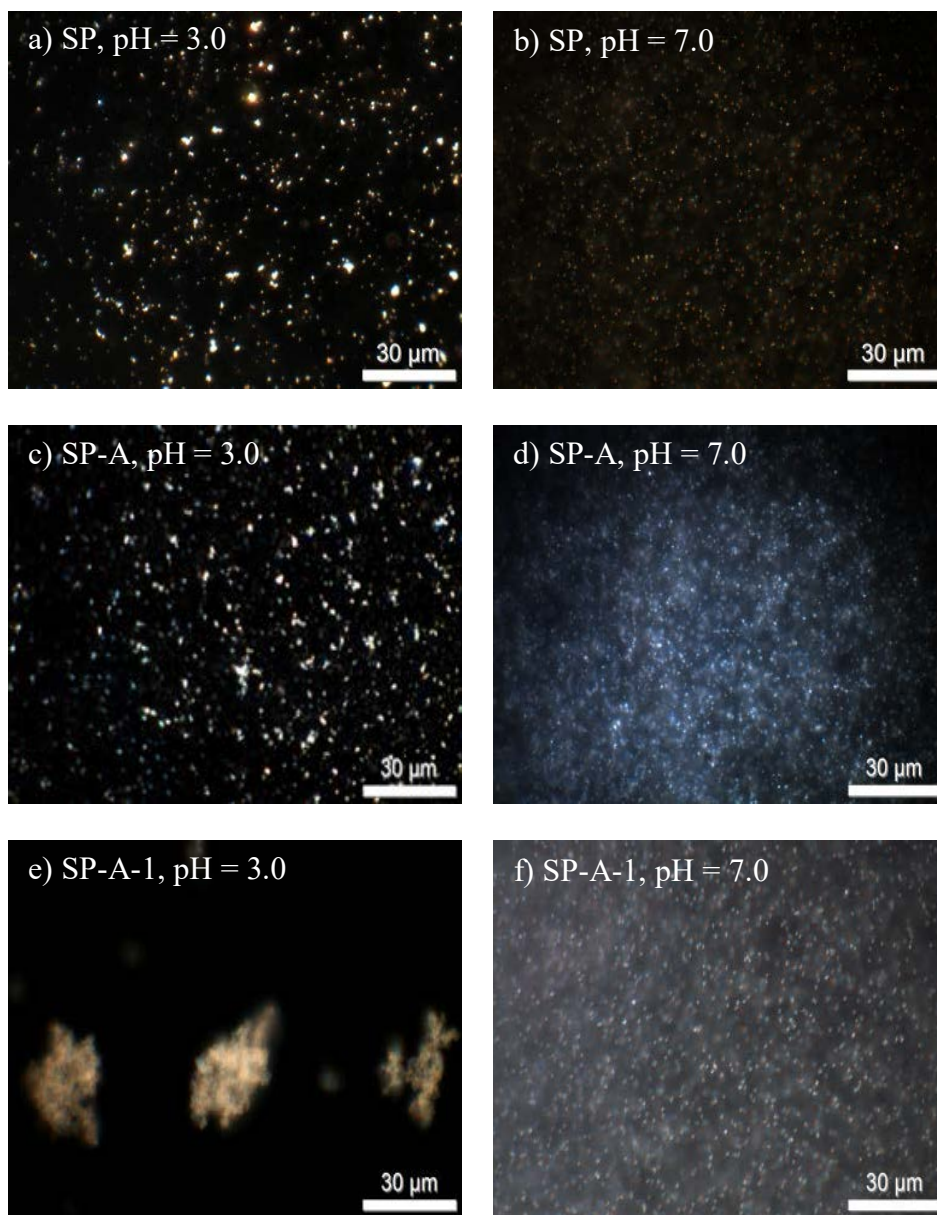


**Figure 1.** Dark field optical microscopy micrographs showing the aggregation state, as a function of pH (3.0 or 7.0), of SP (a, b), SP-A (c, d), and SP-A-1 (e, f) particles.

Grafting APTMS at the surface of SP changes their electrostatic surface potential (**Table 2**) and their state of aggregation (**Figure 1c and d**). **Table 3** reports arithmetic mean diameter  $\pm$  mean absolute deviation, as a function of particle type – the size distributions are reported in **Figure S4**. For SP-A, at pH 3.0 (**Figure 1c**), the aggregates' average diameter ( $D = 1.5 \pm 0.9 \mu\text{m}$ , **Table 3**) is

comparable to unmodified SP particles ( $D = 1.7 \pm 1.0 \mu\text{m}$ ), SP-B and SP-C particles ( $D = 0.9 \pm 0.4 \mu\text{m}$  and  $D = 0.8 \pm 0.5 \mu\text{m}$ , respectively). At pH 7.0, the presence of APTMS at the surface increases the average aggregate size (**Figure 1d**), as compared to unmodified SP at pH 7.0, due to the low zeta potential value.

$D$  approximately increases by an order of magnitude, at pH 3.0, when SA is subsequently grafted onto the particles' surface (**Figure 1e, Table 3**), as compared to unmodified particles (**Figure 1a**, see also **Figure S5**) – the effect is quite striking. At pH 7.0 however (**Figure 1f**), SA grafted particles form much smaller aggregates ( $D = 1.3 \pm 0.3 \mu\text{m}$ ) due to the deprotonation of SA carboxylate groups.

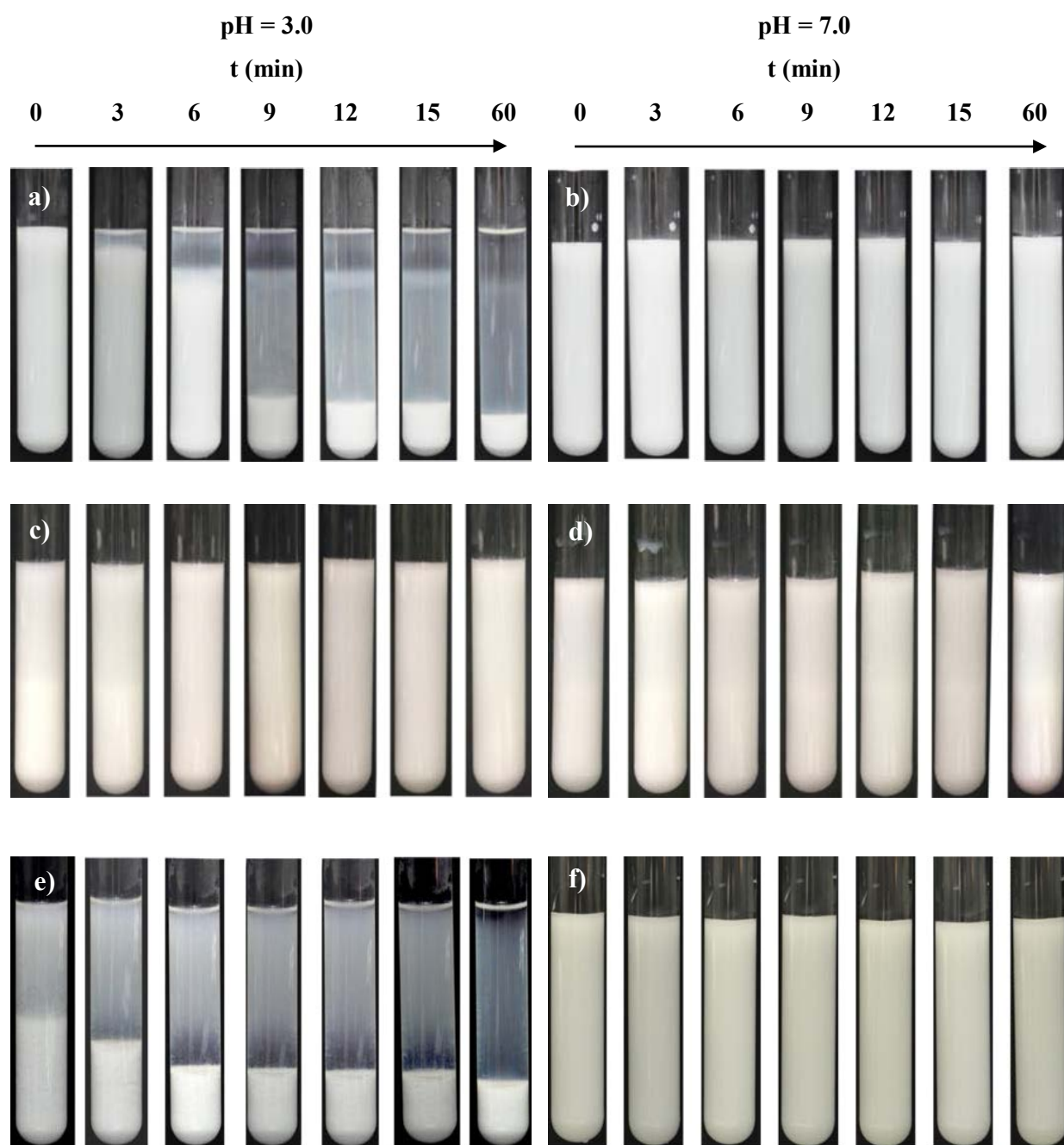
**Table 3.** Average aggregate diameter  $D$  as a function of particle type, at pH 3.0 (N = number of analyzed aggregates).

Particle type	Aggregate average diameter $D$ ( $\mu\text{m}$ )	Average number of particles per aggregate <sup>a</sup>
SP	$1.7 \pm 1.0$ (N = 659)	182
SP-A	$1.5 \pm 0.9$ (N = 917)	128
SP-B	$0.9 \pm 0.4$ (N = 3634)	28
SP-C	$0.8 \pm 0.5$ (N = 1979)	22
SP-A-1	$17 \pm 10$ (N = 231)	$18.2 \times 10^4$
SP-B-2	$12 \pm 7$ (N = 1124)	$5.8 \times 10^4$
SP-C-2	$12 \pm 8$ (N = 915)	$6.4 \times 10^4$

<sup>a</sup>average number of particles per aggregate was obtained from  $(D_{\text{aggregate}}/D_{\text{particle}})^3$

### 3.3 Sedimentation Kinetics

**Figure 2** displays the sedimentation behavior of SP, SP-A and SP-A-1 particles dispersed in water at pHs 3.0 and 7.0, respectively. At pH 3.0, SP particles display a clear sedimentation onset after 3 min – the process is fast for the first 9 min, and then slows down since most of the particles have then sedimented. In contrast, no sedimentation is observed at pH 7.0 even after 60 min (**Figure 2a and b**). This difference is consistent with the measured  $\zeta$  values. SP-A particles do not display any significant sedimentation over the whole duration of the experiment, for both pHs tested (**Figure 2 c and d**). At pH 3.0, the positively charged protonated amino groups' repulsive forces lead to a stable dispersed state, while at pH 7.0 the remaining negatively charged deprotonated hydroxyl groups stabilize the dispersion. However, as the surface density of APTMS increases (SP-B and SP-C), sedimentation occurs at pH 7.0 (results not shown).



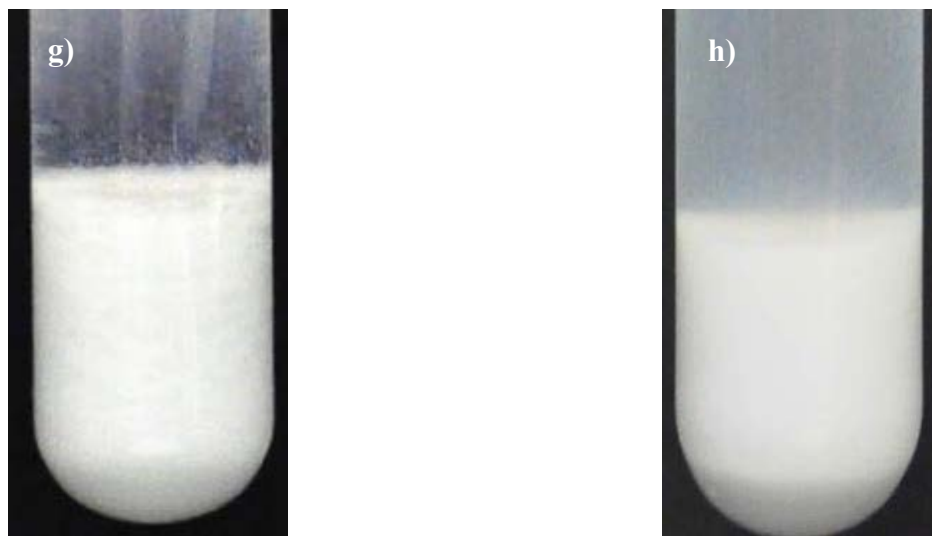


**Figure 2.** Pictures of the sedimentation process (height of test tube = 15.3 cm) for SP (a, b), SP-A (c, d), and SP-A-1 (e, f) particles over 60 min at pHs 3.0 and 7.0 respectively; g, h) close-ups of SP-A-1 and SP sedimented particles, showing a clear difference in particle texture. Additional results for SP-B-2 and SP-C-2 particles are displayed in Figure S6.

For SP-A-1 particles, shown in **Figure 2e-f**, sedimentation starts right away at pH 3.0 and after 3 minutes, it is already fairly advanced. After 6 min, the process significantly slows down, whereas at pH 7.0, SP-A-1 particles stay well dispersed for the whole duration of the experiment, as shown in **Figure 2f**. Note that a similar behavior was observed for SP-B-2 and SP-C-2 particles (results not shown). Another distinct feature is the “grainy” texture of the sedimented SP-A-1 particles (**Figure 2g**), as compared to unmodified SP particles (**Figure 2h**) – indicating the presence of large aggregates at pH 3.0, which is not the case for SP particles.

### 3.4 Kinetic test by UV-Visible spectroscopy

**Figure 3** displays the normalized UV-Vis transmittance results  $T$  of the solutions during 60 min, right after processing, at both pHs 3.0 and 7.0. The results at pH 3.0 were fitted with power laws ( $T = A + B \exp(-t/C)$ ). SP particles sediment moderately fast at pH 3.0 (as indicated by the initial

transmittance slope ( $-B/C$ ) = 0.03,  $R^2 = 0.98$ ), while no net sedimentation is detected at pH 7.0 ( $T$  = 0). These results are consistent with the behavior expected based on zeta potential results (**Table 1**) and visual observations (**Figure 2**). After  $\approx 35$  min,  $T$  has increased up to 50 % for SP particles, and to 60 % after 60 min, with sedimentation still in progress. In contrast, sedimentation is occurring significantly faster at pH 3.0 for SA modified particles (initial slope ( $-B/C$ ) = 0.22 ( $R^2 = 0.98$ ), 0.22 ( $R^2 = 0.95$ ) and 0.07 ( $R^2 = 0.98$ ) for SP-A-1, SP-B-2 and SP-C-2 particles respectively). For SP-A-1,  $T$  increases up to 50 % after only  $\approx 5$  min, and reaches a plateau value of nearly 90 % after 30 min. Similar results are obtained for SP-B-2 particles, while SP-C-2 particles show a slower sedimentation process compared to SP-A-1 and SP-B-2, but still faster compared to SP. Finally, note that all solutions at pH 7.0 displayed no significant UV-Vis  $T$  increase.

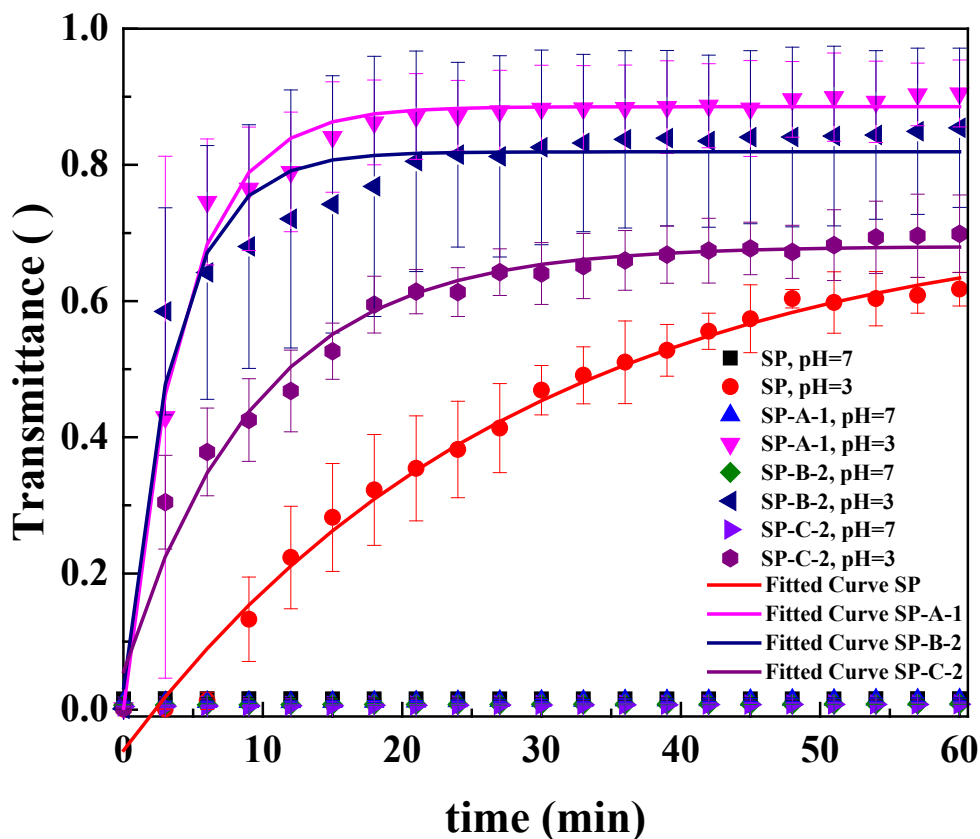


**Figure 3.** Normalized transmittance  $T$  as a function of time for SP, SP-A-1, SP-B-2 and SP-C-2 particles at pH 3.0 and 7.0, and fitted curves for SP, SP-A-1, SP-B-2 and SP-C-2 particles at pH 3.0 over 60 min.

### 3.5 Aggregation/disaggregation Reversibility

**Figure 4** illustrates the reversible nature of the aggregation process for SP and SP-A-1 particles over 4 pH-swing cycles using UV-Vis spectroscopy, starting at pH 7.0, for 60 min. After that time, the pH is decreased to 3.0 for 60 min, and the cycle is repeated 3 other times. Both SP-A-1 and SP particles are able to aggregate and disaggregate reversibly over the course of the 4 tested cycles. At pH 3.0, SP-A-1 particles sediment rapidly within minutes and form aggregates, with UV

transmittance reaching a maximum near 90% each time the pH is brought down to 3.0. When the pH is increased to 7.0 and the solution is sonicated, the dispersion remains stable ( $T \approx 0\%$ ).

SP particles also display a reversible aggregation behavior, but the maximum transmittance after 60 min never goes over 60% - in fact, it decreases as the process is repeated. Furthermore, slight aggregation is also observed at pH 7.0 as the process is repeated. It should be noted however that if the pH is just increased without any sonication, the disaggregation process is very slow.

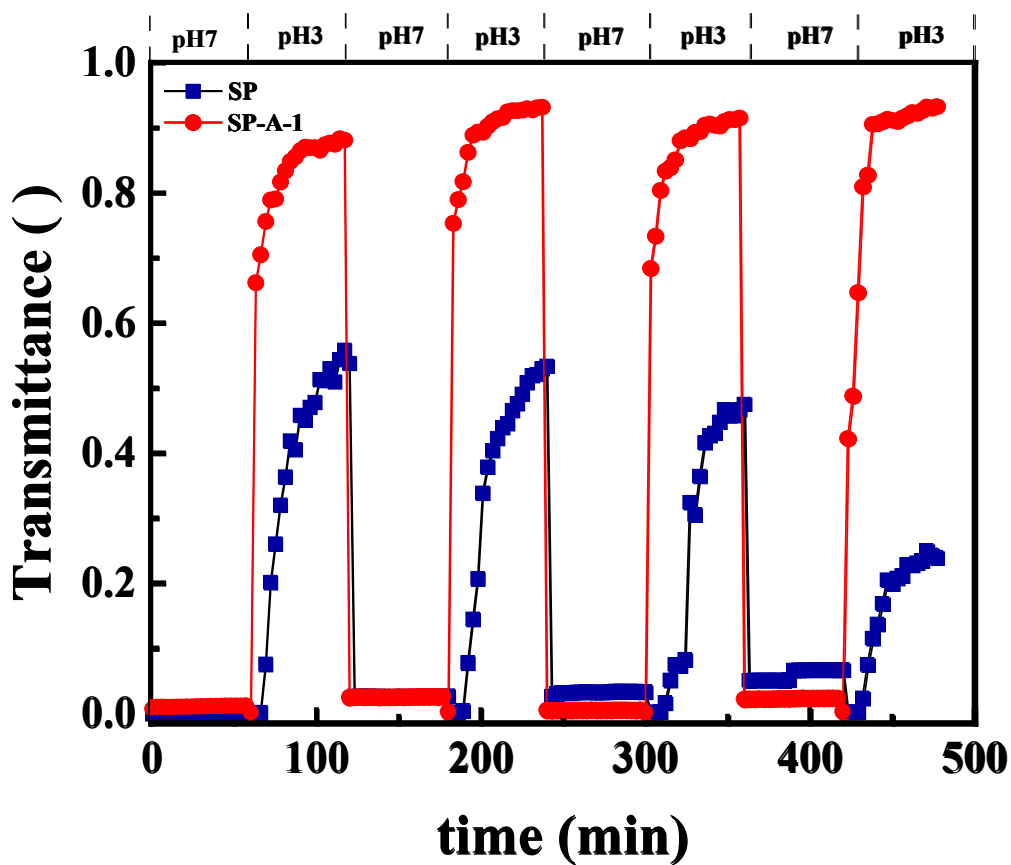


**Figure 4.** Reversibility test for SP (■) and SP-A-1 particles (●) over 4 cycles, during which the pH jumps back and forth from 7.0 to 3.0.

## 4. Discussion

The  $\zeta$  measurements, along with the XPS and FTIR results, confirm that the SP particles have been modified sequentially with covalently grafted APTMS and SA. The average diameter of individual silica particles is  $d \approx 300$  nm - in contrast, the average diameter  $D$  of particle aggregates at pH 3.0, for SA modified particles, is about 10 times superior as compared to aggregates of unmodified particles. Since the volume of an aggregate  $\sim D^3$ , there is approximately  $10^3$  more particles in an aggregate of SA modified particles as compared to an aggregate comprising unmodified particles, as reported in the third column of **Table 3** – a significant difference.

We propose that the main mechanism leading ultimately to the reversible, enhanced aggregation properties of SA modified particles, compared to unmodified particles, originates from hydrogen bonding between neighboring particles grafted with SA. At pH 7.0, SA carboxylic acid groups are deprotonated and maintain the particles in suspension. However, once the pH is brought down to 3.0, the carboxylate groups are protonated and  $\zeta$  is in-between 0-10 mV, which leads to an unstable suspension and particle agglomeration. This gives rise to SA intermolecular interactions via hydrogen bonding, enhancing aggregate formation. Recently, Chen et al. (K. Chen et al., 2017) used SA-modified nanoparticles to prepare pH-sensitive Pickering emulsions. Their work demonstrated that SA significantly alters the emulsions' rheological behavior due to pH-dependent interparticle interactions.

**Figure 5a and b** illustrate the effect of urea on alginate association in solution at pHs 7.0 and 3.0, respectively. Urea is a well-known hydrogen bond disruptor, which should then limit or inhibit hydrogen bonding and aggregate formation. At pH 7.0, urea has no visible effect on solution

turbidity. However, when the pH is brought down to 3.0, alginate phase separate (and can ultimately form a gel when the SA concentration is high enough), a phenomena that is not observed when urea is added to the solution.

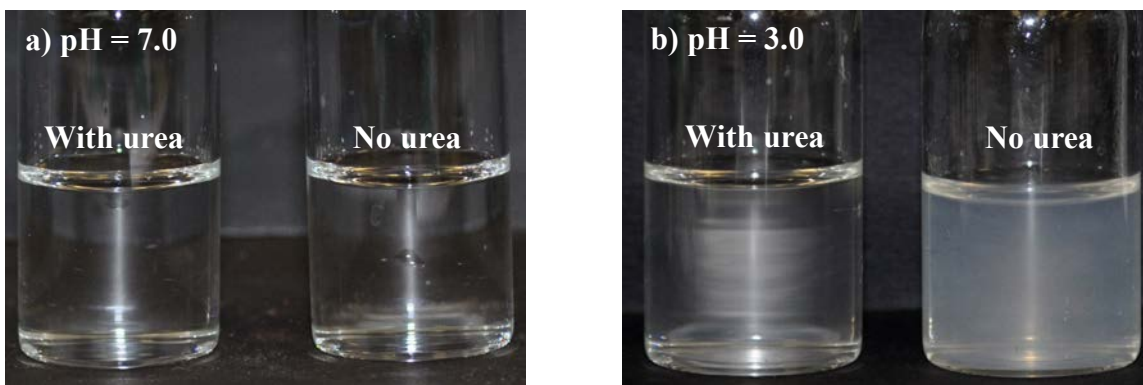


**Figure 5.** Pictures of 0.5 % solution of pure SA in DI water at pH 7.0 (a) and at pH 3.0 (b), with and without urea (16 M). Solution with urea at pH 3.0 remains clear, while without urea it becomes turbid.

Furthermore, investigating the effect of SA molecular weight and architecture (guluronic/mannuronic ratio), and other gelling polysaccharides, is currently in progress.

## 5. Conclusion

This article demonstrates that submicrometer silica particles functionalized with a pH sensitive polysaccharide, sodium alginate, display enhanced aggregation properties at low pH, and reversible aggregation/disaggregation properties in aqueous solutions. The aggregation properties are due to interparticle hydrogen bonding between neighboring sodium alginate modified particle. The particles surface modification was characterized by zeta potential measurements, XPS and FTIR analyses, and UV-Vis was used to characterize the sedimentation kinetics. The results

illustrate how stimuli sensitive surface modified particles can be used as a potential approach to facilitate the aggregation of particles, and to ease separation processes.

**Supporting Information.** Silica particles SEM micrographs, XPS and FTIR spectra of unmodified and modified particles; particle aggregates size distribution; optical microscopy and sedimentation test results.

## AUTHOR INFORMATION

### Corresponding Author

\*(N.V.) Telephone: 514-340-4711 #4524. FAX: 514-340-4152. E-mail: [nick.virgilio@polymtl.ca](mailto:nick.virgilio@polymtl.ca)

### Author Contributions

The manuscript was written through contributions of all authors. All authors have given approval to the final version of the manuscript.

## ACKNOWLEDGMENT

We acknowledge the financial support of Imperial Oil through a University Research Award grant, the Total company, the National Sciences and Engineering Research Council (Discovery Grant), CREPEC (Projet Structurant), Polytechnique Montreal (UPIR undergraduate research grants) and the Canada Foundation for Innovation (John R. Evans Leaders Fund). We would like to thank Dr. Donya Farhanian and Dr. Josianne Lefebvre for performing XPS experiments, Mr. Wendell Raphael for optical microscopy observations, Dr. Benoît Liberelle, Mr. Chang-Sheng Wang, Mr.

Philippe Leclerc, Dr. David Vidal and Mr. David Brassard and Ms. Claire Cerclé for fruitful discussions and technical support.

## References

- Abreu, C. M., Paula, H. C., Seabra, V., Feitosa, J. P., Sarmiento, B., & de Paula, R. C. (2016). Synthesis and characterization of non-toxic and thermo-sensitive poly(N-isopropylacrylamide)-grafted cashew gum nanoparticles as a potential epirubicin delivery matrix. *Carbohydrate Polymers*, 154, 77-85.
- Arkles, B. (2006). Silane Coupling Agents: Connecting Across Boundaries. In I. Gelest (Ed.).
- Bakhteeva, I. A., Medvedeva, I. V., Uimin, M. A., Byzov, I. V., Zhakov, S. V., Yermakov, A. E., & Shchegoleva, N. N. (2016). Magnetic sedimentation and aggregation of Fe<sub>3</sub>O<sub>4</sub>@SiO<sub>2</sub> nanoparticles in water medium. *Separation and Purification Technology*, 159, 35-42.
- Bakumov, V., & Kroke, E. (2008). Polysilazane-induced aggregation of hydrophobic silver colloids. *Langmuir*, 24(19), 10709-10716.
- Ballauff, M., & Lu, Y. (2007). "Smart" nanoparticles: Preparation, characterization and applications. *Polymer*, 48(7), 1815-1823.
- Binks, B. P., Murakami, R., Armes, S. P., & Fujii, S. (2005). Temperature-induced inversion of nanoparticle-stabilized emulsions. *Angewandte Chemie International Edition*, 44(30), 4795-4798.
- Borkovec, M., & Papastavrou, G. (2008). Interactions between solid surfaces with adsorbed polyelectrolytes of opposite charge. *Current Opinion in Colloid and Interface Science*, 13(6), 429-437.
- Chai, L. Y., Yan, X., Li, Q. Z., Yang, B. T., Wang, X., & Wang, Q. W. (2015). Enhancement of ZnO particles aggregation and sedimentation using polysaccharide and amino acid:

432 Importance in abiological granular sludge (ABGS) formation. *Separation and Purification*  
433 *Technology*, 151, 66-73.

434 Chen, K., Yu, G., He, F., Zhou, Q., Xiao, D., Li, J., & Feng, Y. (2017). A pH-responsive emulsion  
435 stabilized by alginate-grafted anisotropic silica and its application in the controlled release  
436 of lambda-cyhalothrin. *Carbohydrate Polymers*, 176, 203-213.

437 Chin, C. J., Yiacoumi, S., & Tsouris, C. (2001). Probing DLVO forces using interparticle magnetic  
438 forces: Transition from secondary-minimum to primary-minimum aggregation. *Langmuir*,  
439 17(20), 6065-6071.

440 Doshi, B., Repo, E., Heiskanen, J. P., Sirvio, J. A., & Sillanpaa, M. (2017). Effectiveness of N,O-  
441 carboxymethyl chitosan on destabilization of Marine Diesel, Diesel and Marine-2T oil for  
442 oil spill treatment. *Carbohydrate Polymers*, 167, 326-336.

443 Durand-Gasselin, C., Sanson, N., & Lequeux, N. (2011). Reversible controlled assembly of  
444 thermosensitive polymer-coated gold nanoparticles. *Langmuir*, 27(20), 12329-12335.

445 Giani, G., Fedi, S., & Barbucci, R. (2012). Hybrid Magnetic Hydrogel: A Potential System for  
446 Controlled Drug Delivery by Means of Alternating Magnetic Fields. *Polymer*, 4(2), 1157-  
447 1169.

448 Harnsilawat, T., Pongsawatmanit, R., & McClements, D. J. (2006). Characterization of beta-  
449 lactoglobulin-sodium alginate interactions in aqueous solutions: A calorimetry, light  
450 scattering, electrophoretic mobility and solubility study. *Food Hydrocolloids*, 20(5), 577-  
451 585.

452 Hemraz, U. D., Lu, A., Sunasee, R., & Boluk, Y. (2014). Structure of poly(N-isopropylacrylamide)  
453 brushes and steric stability of their grafted cellulose nanocrystal dispersions. *Journal of*  
454 *Colloids and Interface Science*, 430, 157-165.

455 Hosseini, A., Zare, E., Ayatollahi, S., Vargas, F. M., Chapman, W. G., Kostarelos, K., &  
 456 Taghikhani, V. (2016). Electrokinetic behavior of asphaltene particles. *Fuel*, 178, 234-242.  
 457 Jia, X., Zhao, X., Tian, K., Zhou, T. T., Li, J. G., Zhang, R. N., & Liu, P. (2016). Novel fluorescent  
 458 pH/reduction dual stimuli-responsive polymeric nanoparticles for intracellular triggered  
 459 anticancer drug release. *Chemical Engineering Journal*, 295, 468-476.  
 460 Kawaguchi, S. T. a. H. (2008). Thermosensitive Pickering Emulsion Stabilized by Poly(N-  
 461 isopropylacrylamide)-Carrying Particles. *Langmuir*, 24(7), 3300-3305.  
 462 Knoblich, B., & Gerber, T. (2001). Aggregation in SiO<sub>2</sub> sols from sodium silicate solutions.  
 463 *Journal of Non-Crystalline Solids*, 283(1-3), 109-113.  
 464 Lattuada, M., & Hatton, T. A. (2007). Functionalization of monodisperse magnetic nanoparticles.  
 465 *Langmuir*, 23(4), 2158-2168.  
 466 Leudjo Taka, A., Pillay, K., & Yangkou Mbianda, X. (2017). Nanosponge cyclodextrin  
 467 polyurethanes and their modification with nanomaterials for the removal of pollutants from  
 468 waste water: A review. *Carbohydrate Polymers*, 159, 94-107.  
 469 Mohammadi, S., Rashidi, F., Mousavi-Dehghani, S. A., & Ghazanfari, M. H. (2016). Modeling of  
 470 asphaltene aggregation phenomena in live oil systems at high pressure-high temperature.  
 471 *Fluid Phase Equilibria*, 423, 55-73.  
 472 Morelli, S., Holdich, R. G., & Dragosavac, M. M. (2016). Chitosan and Poly (Vinyl Alcohol)  
 473 microparticles produced by membrane emulsification for encapsulation and pH controlled  
 474 release. *Chemical Engineering Journal*, 288, 451-460.  
 475 Noel, S., Liberelle, B., Robitaille, L., & De Crescenzo, G. (2011). Quantification of primary amine  
 476 groups available for subsequent biofunctionalization of polymer surfaces. *Bioconjugate*  
 477 *Chemistry*, 22(8), 1690-1699.

478 Ohki, S., & Ohshima, H. (1999). Interaction and aggregation of lipid vesicles (DLVO theory  
 479 versus modified DLVO theory). *Colloids and Surfaces B-Biointerfaces*, 14(1-4), 27-45.

480 Pickering, K. L., Khimi, S. R., & Ilanko, S. (2015). The effect of silane coupling agent on iron  
 481 sand for use in magnetorheological elastomers Part 1: Surface chemical modification and  
 482 characterization. *Composites Part A Applied Science and Manufacturing*, 68, 377-386.

483 Qiao, P., Niu, Q. S., Wang, Z. B., & Cao, D. P. (2010). Synthesis of thermosensitive micelles  
 484 based on poly(N-isopropylacrylamide) and poly(L-alanine) for controlled release of  
 485 adriamycin. *Chemical Engineering Journal*, 159(1-3), 257-263.

486 Rahelivao, M. P., Andriamanantoanina, H., Heyraud, A. & Rinaudo, M. (2013). Structure and  
 487 properties of three alginates from Madagascar seacoast algae. *Food Hydrocolloids*, 32,  
 488 143-146.

489 Rodgers, A. N., Velicky, M., & Dryfe, R. A. (2015). Electrostatic Stabilization of Graphene in  
 490 Organic Dispersions. *Langmuir*, 31(48), 13068-13076.

491 Stular, D., Jerman, I., Naglic, I., Simoncic, B., & Tomsic, B. (2017). Embedment of silver into  
 492 temperature- and pH-responsive microgel for the development of smart textiles with  
 493 simultaneous moisture management and controlled antimicrobial activities. *Carbohydrate*  
 494 *Polymers*, 159, 161-170.

495 Verwey, E. J. (1947). Theory of the stability of lyophobic colloids. *Journal of Physical and Colloid*  
 496 *Chemistry*, 51(3), 631-636.

497 Wang, C. S., Natale, G., Virgilio, N., & Heuzey, M. C. (2016). Synergistic gelation of gelatin B  
 498 with xanthan gum. *Food Hydrocolloids*, 60, 374-383.

499 Wu, B. C., & McClements, D. J. (2015). Design of reduced-fat food emulsions: Manipulating  
500 microstructure and rheology through controlled aggregation of colloidal particles and  
501 biopolymers. *Food Research International*, 76(Pt 3), 777-786.

502 Xu, X. B., Lu, S. Y., Gao, C. M., Wang, X. G., Bai, X., Duan, H. G., Liu, M. Z. (2015). Polymeric  
503 micelle-coated mesoporous silica nanoparticle for enhanced fluorescent imaging and pH-  
504 responsive drug delivery. *Chemical Engineering Journal*, 279, 851-860.

505 Yan, Y., Seeman, D., Zheng, B., Kizilay, E., Xu, Y., & Dubin, P. L. (2013). pH-Dependent  
506 aggregation and disaggregation of native beta-lactoglobulin in low salt. *Langmuir*, 29(14),  
507 4584-4593.

508

509